The EUROfusion JET-ILW pedestal database

L. Frassinetti[1], S. Saarelma[2], F. Imbeaux[3], G. Verdoolaege[4,5], P. Bilkova[6], P. Bohm[6], R. Fridström[1], E. Giovannozzi[7], M. Owsiak[8], M. Dunne[9], B. Labit[10], R. Scannell[2], J.C. Hillesheim[2] and JET contributors[11*]

[1]*Division of Fusion Plasma Physics, KTH Royal Institute of Technology, Stockholm SE*
[2] *CCFE, Culham Science Centre, Abingdon, Oxon OX14 3DB, UK*
[3]*CEA, IRFM, F-13108 Saint-Paul-lez-Durance, France*
[4]*Department of Applied Physics Ghent University Sint-Pietersnieuwstraat 41 B-9000 Ghent, Belgium*
[5]*Laboratory for Plasma Physics—Royal Military Academy, Avenue de la Renaissancelaan 30, Brussels, Belgium*
[6] *Institute of Plasma Physics of the CAS, Za Slovankou 3, 182 00 Prague 8, Czech Republic*
[7]*ENEA, Fusion and Nuclear Safety Department, Via E. Fermi 45, 00044 Frascati, Italy*
[8]*Poznan Supercomputing and Networking Center, IChB PAS, Noskowskiego 12/14, Poznan, Poland*
[9]*Max-Planck-Institut für Plasmaphysik, Garching, Germany*
[10]*Swiss Plasma Center (SPC), Ecole Polytechnique Fédérale de Lausanne (EPFL), Lausanne,Switzerland*
[11]*EUROfusion Consortium, JET, Culham Science Centre, Abingdon, OX14 3DB, UK*
** see X. Litaudon et al., Nuclear Fusion 57, 102001 (2017)*

1. Introduction

To enhance the scientific output of multi-machine comparisons, EUROfusion has promoted the creation of several databases with common definitions and with a common platform. The databases will be stored into the IMAS format (ITER integrated modelling and analysis suite) [1]. This work is a concise overview of the EUROfusion pedestal database of JET-ILW, briefly discussing (a) technical aspects of the work, such as the selection rules, (b) the initial analysis, aimed at verifying that the database produces reasonable results and (c) the scaling of the thermal stored energy near the pedestal top of JET-ILW.

2. Fitting procedure and data selection.

The pedestal structure is determined using the pre-ELM profiles (70-99% of the ELM cycle) of the High Resolution Thomson Scattering [2] processed as described in [3]. Pedestal parameters are extracted by fitting the experimental data with both a *mtanh* function [4] and a combination of linear functions. In the JET-ILW database, the two fitting functions produce qualitatively similar results. Due to uncertainty in the absolute position of the Thomson data, the profiles have been systematically shifted to have 100eV at the separatrix, as estimated using the two point model for the power balance at the separatrix.

To ensure a good quality of the pedestal data, the entries of the JET-ILW pedestal database have been selected accordingly to the following three rules. (a) The reduced χ^2 of the fits calculated in the region $0.8<\psi_N<1.05$ must be lower than 1.5 to ensure good fits. (b) The time intervals must be stationary for at least 0.5s and (c) for at least $2\tau_E$. The stationarity has been verified in several global parameters: I_p, q_{95}, NBI power, ICRH power, radiated power, strike point position, gas fuelling rate, seeding rate, line integrated density, triangularity, β_N, H_{98}, ELM frequency. The level of stationarity cannot be strictly determined and must be relatively flexible. Several discharges have been performed with engineering parameters in feedback (for example, on gas to keep f_{ELM} constant or on the NBI power to keep β_N constant).

Version 1 of the JET-ILW database contains ≈1050 entries. Details on the selection rules, definitions and workflow can be found at the link in reference [5].

3. ELM type

A key distinction to be included in the database is the ELM type. The data have been labelled considering only two type of ELMs, type I and type III. ELMs are defined as type I when their frequency (f_{ELM}) increases with increasing P_{sep} (power through the separatrix) with all other engineering parameters constant, while are defined as type III when the frequency decreases with increasing P_{sep} [6].

It is very challenging to apply this empirical definition to the database. Figure 1 shows f_{ELM} versus P_{sep}. P_{sep} has been estimated as total input power minus the inter-ELM radiated power. No clear trend is observed when considering the entire database. Therefore, the data have been divided in many subsets with constant engineering parameters (apart from power). The red data show an example at 3MA and the orange data an example at 2MA. In both cases, the ELMs have been classified as Type I. The blue data show a specific NBI power scan at 1.4MA/1.7T [7]. The ELM frequency decreases till $P_{sep}\approx$4MW, highlighting Type III ELMs. At higher P_{sep}, this scan is characterized by Type I ELMs.

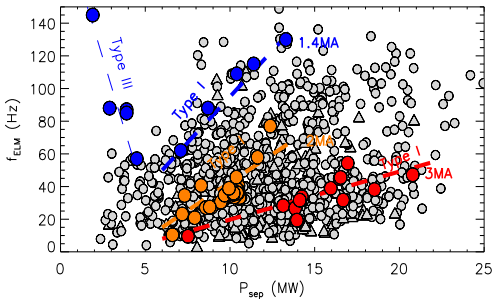

Figure 1. ELM frequency vs P_{sep}. Light blue: NBI power scan at 1.4MA/1.7T. Orange and red data: datasets with constant engineering parameters (apart P_{sep}) at I_p=2MA, and I_p=3MA respectively.

We must highlight that this approach cannot be 100% reliable and it is possible that some entries have been labelled with the wrong ELM type.

4. Pedestal height and pedestal width

The pre-ELM pedestal height determined from *mtanh* fit for electron density and temperature is shown in figure 2. Hereafter, only deuterium plasmas with no pellets, no seeding, no kicks, no RMPs are considered, unless otherwise stated. The colors highlight the total input power determined as $P_{net}=P_{NBI}+P_{ICRH}+P_{\Omega}-P_{shi}$.

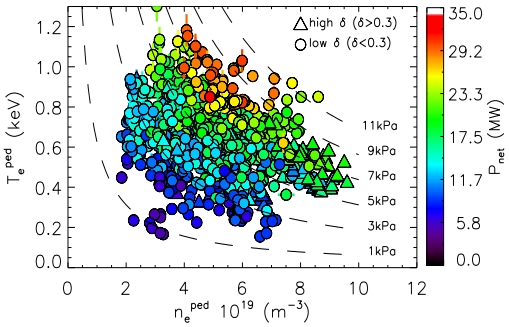

Figure 2. Pedestal temperature and density for deuterium unseeded plasmas. Dashed lines highlight the isobars.

First of all, high triangularity (δ) plasmas tend to have higher pedestal density, in agreement with many previous results [8]. Then, we can observe that the increase in P_{net} leads to the increase in the pedestal pressure. This is mainly due the increase of the pedestal temperature (T_e^{ped}) . This is also in agreement with previous JET-ILW results [7,9].

The pre-ELM pedestal width is determined from the *mtanh* fit of the experimental data for temperature and density. Due to the lack of a deconvolution method for the electron pressure (p_e), the p_e width is estimated in two ways: (a) by fitting the product of the deconvolved T_e and n_e fits and (b) using the EPED definition [10], $w_{pe}=(w_{Te}+w_{ne})/2$. The width from definition (b) is shown in figure 3. It is clear that w_{pe} does not follow the trend expected from the EPED1 model, $w_{pe}=0.076(\beta_\theta^{ped})^{0.5}$. This might be due to a variation in the coefficient 0.076 rather than a change in the exponent.

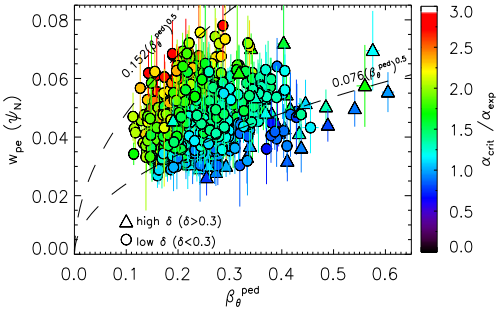

Figure 3. Width of the p_e pedestal (using the EPED definition) versus the total poloidal beta at the pedestal. Colors highlight the distance from the P-B boundary, estimated as $\alpha_{crit}/\alpha_{exp}$.

5. Pedestal stability, normalized pressure gradient and pedestal position.

To complement the experimental data, the database contains the results of the peeling-ballooning (P-B) stability analysis. This was done by self-consistent runs of ELITE [11] (using the bootstrap current from the Sauter model [12]), which provide the normalized

pressure gradient α and the pedestal temperature expected by the P-B stability, α_{crit} and T_e^{crit} respectively. These parameters are useful to determine how close the plasma is to the P-B boundary, for example by comparing α_{crit} with the experimental α (α_{exp}). The normalized pressure gradient is defined as in reference [13].

It turns out that when JET-ILW is close to the P-B boundary (i.e. $0.9<\alpha_{crit}/\alpha_{exp}<1.1$), the pedestal width scales as expected in the EPED1 model. See the "blue" colors in figure 3. The larger the deviation from the scaling $w_{pe}=0.076(\beta_\theta^{ped})^{0.5}$, the larger the distance from the P-B boundary ($\alpha_{crit}/\alpha_{exp}>2.5$, see red colors in figure 3).

Keeping in my mind that the goal of this work is to validate the database (for example by cross-checking trends from earlier works), we have investigated the role of the pedestal position in the pedestal stability. The pedestal position is determined as the position of the maximum gradient.

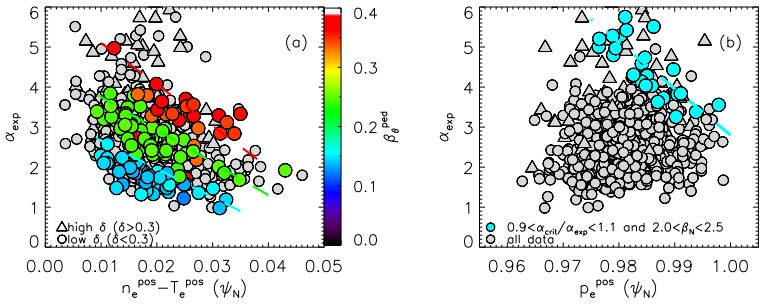

Figure 5. (a) Experimental normalized pressure gradient α_{exp} versus the relative shift for the entire database (grey data) and for data with similar β_θ^{ped} (colors). (b) α_{exp} versus p_e^{pos} for the entire database (grey data) and for low-δ data on the P-B boundary with $2.0<\beta_N<2.5$ (light blue).

Two main results are present in the recent literature regarding the role of the pedestal position. In JET-ILW, it has been found that the increase of normalized pressure gradient α_{exp} is correlated with the reduction of the relative shift (the difference between n_e^{pos} and T_e^{pos}) [14]. In AUG, it has been found that the inward shift of the p_e position (p_e^{pos}) leads to the increase of the pedestal pressure height [15].

Figure 5(a) shows the correlation between α_{exp} and the relative shift. Considering the entire database (grey data), no clear trend is present. However, since β influences the pedestal stability, reference [14] highlights that the trend is present at constant β_θ^{ped}. The colors in figure 5(a) highlight the datasets with $\beta_\theta^{ped}\approx 0.15$ (light blue), $\beta_\theta^{ped}\approx 0.25$ (green) and $\beta_\theta^{ped}\approx 0.35$ (red). The selected datasets shows a trend consistent with reference [14].

Figure 5(b) shows the correlation of α_{exp} versus the pressure position. Considering the entire dataset (grey data), no correlation is present. However, the dependence of the normalized pressure gradient on the p_e^{pos} is a consequence of the P-B stability and is therefore expected only when the plasma reaches the P-B boundary. The data close to the P-B boundary ($0.9<\alpha_{crit}/\alpha_{exp}<1.1$) are highlighted in blue in figure 5(b). Moreover, since the pedestal stability is affected also by β and shape, the blue data have been further selected with low-δ and with $2.0<\beta_N<2.5$. The selected dataset has a trend between α_{exp} and p_e^{pos} consistent with what observed in AUG [15].

6. Scalings of the stored energy at $\psi_N=0.9$.

One of the reasons to create a pedestal database is to update the scaling laws of the pedestal for the extrapolation of the pedestal to unexplored operational regimes or to new machines. In this section we focus only on the pedestal stored energy. To estimate the pedestal stored energy, we have used a simple but practical "proxy", W_{90}. This is calculated as the stored energy at $\psi_N=0.9$ determined from the ELM-averaged total pressure (assuming $T_i=T_e$ and calculating n_i from n_e and Z_{eff} with Be as main impurity). This definition has been applied to a JET-C dataset giving a good agreement with the Cordey scaling [16]. This suggests that W_{90} is a simple but reasonable proxy to have an estimate comparable to the W_{ped} used by Cordey. Moreover, this definition has the advantage of being representative of the stored

energy above the top of the pedestal. Therefore, it can be directly used by the core modellers as reliable "edge" value.

This section show the scaling results using a nonlinear Bayesian regression method with the following parameters: I_p, P_{net}, δ, fuelling rate (Γ). Different regression methods and different sets of parameters will be discussed in future works. Note that parameters such as density or magnetic field cannot be included in the present dataset because of their strong correlation with I_p. Their inclusion will require a multi-machine effort.

Figure 6(a) shows the regression for D plasmas with no N seeding, no RMPs and no kicks. The regression results using the model of equation 1 are reported in table 1.

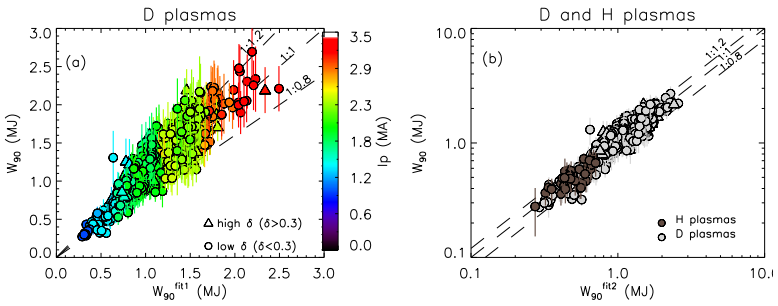

Figure 6. ELM averaged thermal stored energy at ψ_N=0.9 versus empirical fits, (a) considering only D plasmas and (b) considering H and D plasmas.

$$W_{90} = \alpha_0 I_p^{\alpha_I} P_{net}^{\alpha_P} \delta^{\alpha_\delta} \Gamma^{\alpha_\Gamma} \quad (1)$$

The exponents of I_p and P_{net} are slightly lower than those obtained by Cordey, which were respectively α_I *=1.41±0.06* and α_P *=0.5±0.04*. However, the lower α_I might be due to the fact that in equation 1 the density is not considered.

Figure 6(b) shows the regression considering all the data of frame (a) plus the H plasma. In this case, the main ion isotope mass A has been included in the regression. We can note that that inclusion of the hydrogen data does not influence the values of the exponents, suggesting that the result is rather robust. Moreover, we can note that exponent of the isotope is significantly larger than what was obtained in the IPB98(y,2) scaling (which was 0.19), but it is similar to the mass exponent recently determined for the energy confinement in JET-ILW (≈0.4) as shown in reference [17].

	α_0	α_I	α_P	α_δ	α_Γ	α_A
D (fit 1)	*0.33±0.03*	*1.25±0.05*	*0.29±0.03*	*0.33±0.04*	*-0.06±0.01*	-
D and H (fit 2)	*0.21±0.02*	*1.25±0.05*	*0.30±0.03*	*0.30±0.03*	*-0.06±0.01*	*0.48±0.08*

Table 1. Scaling parameters of equation 1 using a nonlinear Bayesian regression method.

7. Conclusions and outlook

The work has briefly described the EUROfusion pedestal database for JET-ILW. A preliminary analysis shows that the results are consistent with previous JET-ILW works, suggesting that the data contained in the database are rather reliable. Future works will investigate the discrepancy between the P-B model and the JET-ILW experimental data and will extend the scaling analysis initiated in Section 6.

Acknowledgment. This work has been carried out within the framework of the EUROfusion Consortium and has received funding from the Euratom research and training programme 2014-2018 under grant agreement No 633053. The views and opinions expressed herein do not necessarily reflect those of the European Commission.

References

[1] F. Imbeaux *et al.*, Nucl. Fusion **55** (2015) 123006.
[2] R. Pasqualotto *et al.*, *Rev. Sci. Instrum.* **75**, 3891 (2004).
[3] L. Frassinetti *et al.*, *Rev. Sci. Instrum.* 83, 013506 (2012)
[4] R. Groebner *et al.*, *Nucl. Fusion* **41** 1789 (2001)
[5]https://users.euro-fusion.org/iterphysicswiki/index.php/Database
[6] Sartori *et al.*, Plasma Phys. Controll. Fus. **46**, 723 (2004)
[7] C. Maggi et al., *et al.*, Nucl. Fus. **55**, 113031 (2015)
[8] M. Beurskens *et al.*, Nucl. Fus. **54**, 043001 (2014)
[9] C. Challis *et al.*, Nucl. Fus. **55**, 053031 (2015)
[10] P.B. Snyder et al., Phys. Plasmas 16 056118 (2009)
[11] S. Saarelma *et al.*, *Phys. Plasmas* **22** 056115 (2015)
[12] O. Sauter *et al.*, *Phys. Plasmas* **6** 2834 (1999)
[13] R. L. Miller R.L. Phys. Plasmas **5** 973 (1998)
[14] E. Stefanikova, Nucl. Fusion **58**, 056010 (2018)
[15] M. Dunne, Plasma Phys.Controll.Fus. **59**, 014017 (2017)
[16] J.C. Cordey et al., Nucl. Fusion **43**, 670 (2003)
[17] C. Maggi Plasma Phys.Controll.Fus. **60**, 014045 (2018)